

# *Fractal-Based Point Processes*

2005

**Steven Bradley Lowen**

*Harvard Medical School  
McLean Hospital*

**Malvin Carl Teich**

*Boston University  
Columbia University*

WILEY

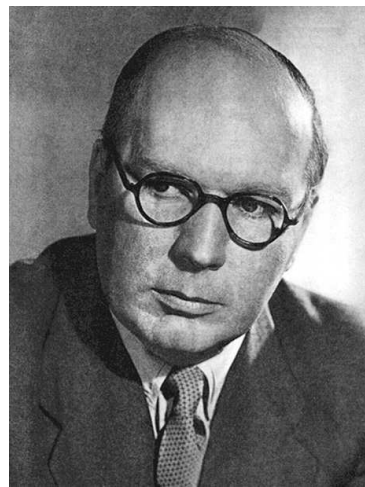
# 10

---

## *Fractal-Shot-Noise-Driven Point Processes*



In 1939, the Polish-born mathematician **Jerzy Neyman (1894–1981)** conceived the “Neyman Type-A” probability distribution and, with Elizabeth Scott in 1958, developed its generalization: the cluster point process.



**Maurice Stevenson Bartlett (1910–2002)**, a British statistician, constructed the shot-noise-driven doubly stochastic Poisson point process and showed that it is a particular Neyman–Scott cluster point process.

<b>10.1 Integrated Fractal Shot Noise</b>	204
<b>10.2 Counting Statistics</b>	205
<b>10.2.1 Counting distribution</b>	205
<b>10.2.2 Count moments</b>	207
<b>10.2.3 Normalized variance</b>	208
<b>10.2.4 Normalized Haar-wavelet variance</b>	210
<b>10.3 Time Statistics</b>	212
<b>10.4 Coincidence Rate</b>	214
<b>10.5 Spectrum</b>	215
<b>10.6 Related Point Processes</b>	216
<b>10.6.1 Point process in the Gaussian limit of fractal shot noise</b>	216
<b>10.6.2 Fractal-shot-noise-driven integrate-and-reset point process</b>	217
<b>10.6.3 Hawkes point process</b>	217
<b>10.6.4 Bartlett–Lewis fractal point process</b>	218
<b>Problems</b>	219

In this chapter we consider two classes of point processes for which fractal shot noise serves as the rate. Fractal shot noise is a continuous stochastic process described in detail in the previous chapter. We focus on a point-process generation mechanism that is Poisson; however, we also briefly consider an integrate-and-reset generation mechanism at the end of the chapter. The properties of these two classes of point processes are closely related, as will become apparent subsequently.

Conceived by Bartlett (1964) in the context of ecology, the **shot-noise-driven doubly stochastic Poisson point process** (abbreviated **shot-noise-driven Poisson process**) results when any form of shot noise serves as the rate for a Poisson-event generator. Bartlett developed a two-dimensional version of this process and recognized it as a particular **Neyman–Scott cluster process** (see Sec. 4.5) comprising Poisson primary and Poisson secondary event sequences [see Neyman & Scott (1958); Vere-Jones (1970); Lawrance (1972)]. An extensive list of applications has come to the fore for this family of point processes, in fields as diverse as entomology, astrophysics, visual science, geophysics, neurophysiology, and photon statistics, among others.<sup>1</sup> The probability distribution that universally emerges in the long counting-time limit, the Neyman Type-A distribution (Neyman, 1939), has also found extensive application.<sup>2</sup>

The generation of this process is schematically illustrated in Fig. 10.1. A primary homogeneous Poisson point process  $dN_1(t)$  with mean rate  $\mu$  comprises the first stage. These events then pass through a linear filter with impulse response function  $h(t)$ .

<sup>1</sup> Examples can be found in Neyman & Scott (1958); Vere-Jones (1970); Neyman & Scott (1972); Teich & Saleh (1981b, 1987, 1988, 1998); Saleh & Teich (1982, 1983); Saleh, Tavoracci & Teich (1981); Teich, Saleh & Peřina (1984).

<sup>2</sup> See, for example, McGill (1967); Teich (1981); Teich & Saleh (1981a, 1987, 2000); Saleh & Teich (1985a); Saleh et al. (1983); Teich, Prucnal, Vannucci, Breton & McGill (1982a,b); Prucnal & Teich (1982); Teich, Tanabe, Marshall & Galayda (1990).

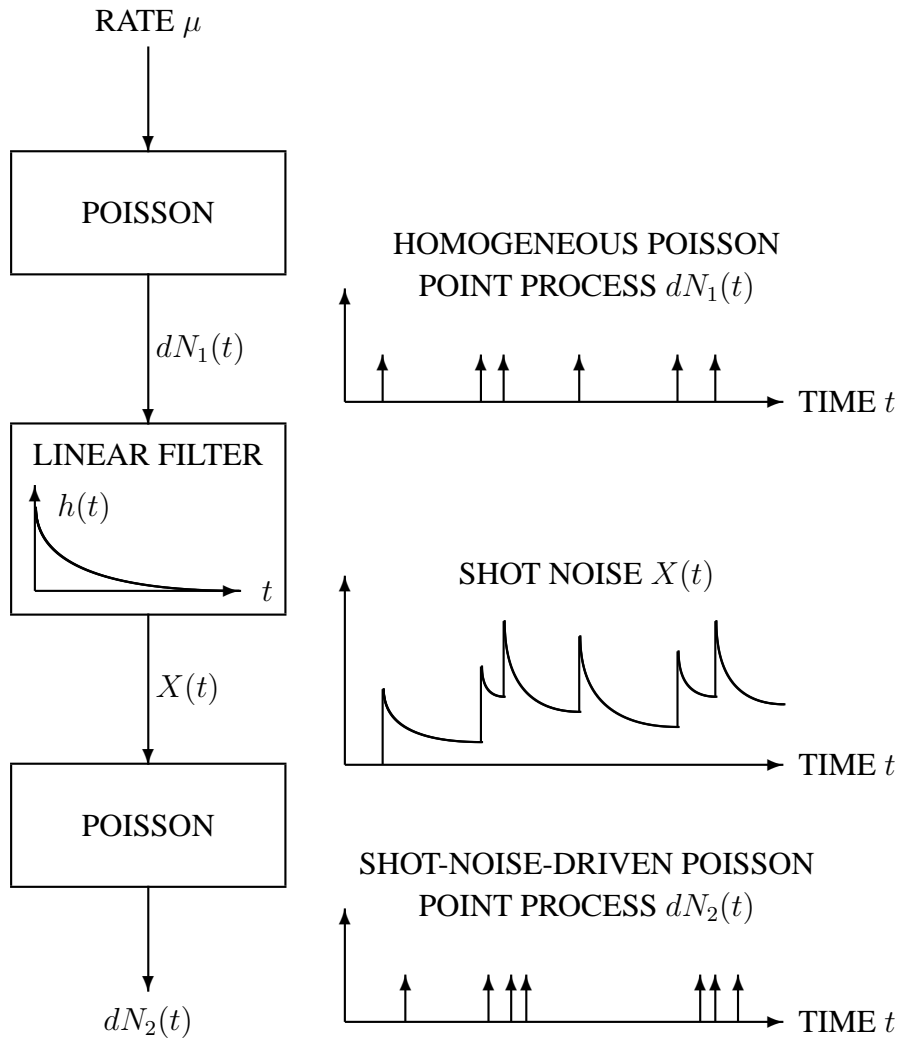


**Fig. 10.1** The shot-noise-driven doubly stochastic Poisson point process arises from two Poisson processes mediated by a linear filter. The quantity  $\mu$  represents the rate of the first Poisson point process,  $h(t)$  is the impulse response function of the linear filter, and  $X(t)$  is the continuous-time shot-noise amplitude at the output of the linear filter. The stochastic process  $X(t)$  serves as the rate function for a second Poisson point process. The overall output  $dN_2(t)$  is a shot-noise-driven doubly stochastic Poisson point process. If  $h(t)$  decays in a power-law fashion,  $X(t)$  is fractal shot noise and  $dN_2(t)$  is a fractal-shot-noise-driven Poisson process.

This filter produces a shot noise  $X(t)$  at its output. This shot noise, in turn, serves as the input to a second Poisson process that generates events  $dN_2(t)$  at the time-varying rate determined by  $X(t)$ . Since the rate of the point process  $dN_2(t)$  coincides with the shot-noise driving process  $X(t)$ ,  $dN_2(t)$  incorporates the variance imparted by this rate and therefore does not belong to the family of homogeneous Poisson point processes. The primary-process rate  $\mu$  and the impulse response function  $h(t)$  completely characterize  $dN_2(t)$ .

In this chapter we develop the properties of the fractal-based form of  $dN_2(t)$ , which is officially known as the **fractal-shot-noise-driven doubly stochastic Poisson point process**, which we abbreviate as the **fractal-shot-noise-driven Poisson process**. In accordance with the results established in Chapter 9, the linear-filter impulse response function decays in a power-law fashion, which gives rise to the fractal-shot-noise stochastic rate  $X(t)$ . The impulse response function  $h(K, t)$  is taken to contain a stochastic component. We can also describe the fractal version of the shot-noise-driven Poisson process in terms of a two-stage **fractal Neyman–Scott cluster process**, in which each event of a primary Poisson point process directly generates a random number of events in a secondary Poisson point process (see Sec. 4.5). The two formulations are isomorphic (see Lowen & Teich, 1991, Appendix A). In the last sections of the chapter, several related processes are briefly described; these include the **fractal-shot-noise-driven integrate-and-reset process**, the **Hawkes point process**, and the **fractal Bartlett–Lewis cascaded process**.

The fractal-shot-noise-driven Poisson process enjoys a broad variety of applications, including the modeling of earthquake occurrence times, Čerenkov photon statistics, diffusion processes, action-potential statistics, and computer network traffic (considered in Secs. 13.5.5 and 13.6). Various applications are discussed by Vere-Jones (1970); Lowen & Teich (1991); Teich et al. (1997, 1990); Ryu & Lowen (1995, 1997, 1998), as well as in the problems at the end of this chapter.

## 10.1 INTEGRATED FRACTAL SHOT NOISE

The time integral of the shot-noise process  $X(t)$  forms an auxiliary random process  $X_T(t)$ ,

$$X_T(t) \equiv \int_t^{t+T} X(u) du. \quad (10.1)$$

Conveniently, the time integral of a shot-noise process forms another shot-noise process, with corresponding impulse response function

$$h_T(K, t) \equiv \int_t^{t+T} h(K, u) du. \quad (10.2)$$

A representative pair of impulse response functions,  $h(t)$  and  $h_T(t)$ , is shown in Fig. 10.2.

The integrated process finds use in establishing the properties of the fractal-shot-noise-driven Poisson process  $dN_2(t)$ . The first-order moment generating function

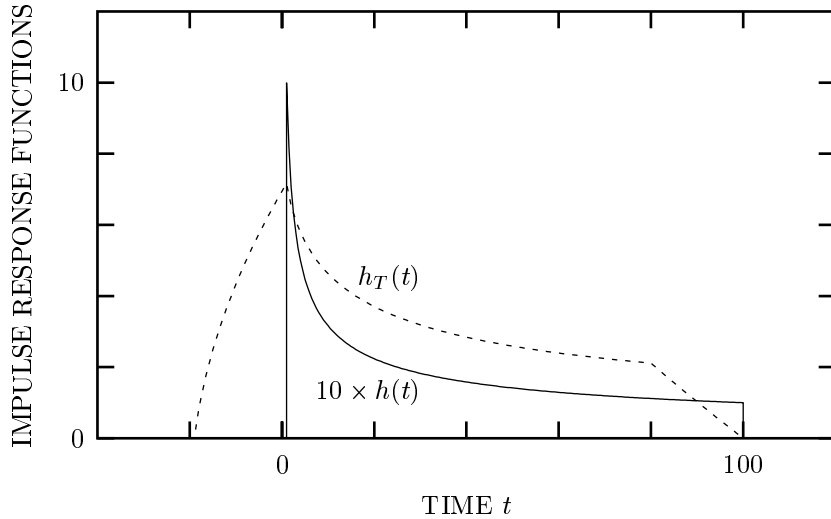


**Fig. 10.2** Representation of a particular power-law-decaying impulse response function,  $h(t)$  ( $\times 10$ ) vs. time  $t$  (solid curve), and its associated integrated impulse response function,  $h_T(t)$  (dotted curve). The parameters are  $\beta = \frac{1}{2}$ ,  $A = 1$ ,  $B = 100$ ,  $K = 1$ , and  $T = 20$ . The integrated version  $h_T(t)$  is derived from  $h(t)$  via Eq. (10.2); for the parameters shown it is proportional to the average of  $h(t)$  over the following 20 time units.

of the integrated shot-noise process  $X_T(t)$  turns out to yield all of the first-order statistics of  $dN_2(t)$ , including its counting and time-interval distributions (Saleh & Teich, 1982). Closed-form results are available for some special cases (Lowen & Teich, 1991, Sec. IIIC and Appendix B).

## 10.2 COUNTING STATISTICS

### 10.2.1 Counting distribution

A recurrence relation provides the counting distribution,  $p_Z(n; T) = \Pr\{Z(T) = n\}$ , for any shot-noise-driven Poisson process (Saleh & Teich, 1982). The first step is to determine the probability of zero events occurring in a specified time duration  $T$ :

$$p_Z(0; T) = \exp\left(\mu E\left[\int_{-\infty}^{\infty} \{\exp[-h_T(K, t)] - 1\} dt\right]\right), \quad (10.3)$$

where the expectation is over  $K$ . For  $n > 0$  we write

$$p_Z(n + 1; T) = \frac{1}{n + 1} \sum_{k=0}^n c_k p_Z(n - k; T), \quad (10.4)$$

where the coefficients  $c_k$  are given by

$$c_k \equiv \frac{\mu}{k!} \mathbb{E} \left[ \int_{-\infty}^{\infty} [h_T(K, t)]^{k+1} \exp[-h_T(K, t)] dt \right]. \quad (10.5)$$

Detailed expressions for the coefficients  $c_k$ , which permit the counting distribution to be calculated, are provided in Sec. A.7.1 for a fractal-shot-noise-driven Poisson process with a deterministic impulse response function.

The **Neyman Type-A counting distribution** emerges from Eqs. (10.3)–(10.5) in the limit of a deterministic, delta-function impulse response function of area  $a$ ,  $h(t) = a \delta(t)$ :

$$p_Z(0; T) = \exp\{\mu T (e^{-a} - 1)\} \quad (10.6)$$

$$p_Z(n+1; T) = \frac{1}{n+1} \mu T \sum_{k=0}^n \frac{a^{k+1} e^{-a}}{k!} p_Z(n-k; T). \quad (10.7)$$

Although this distribution corresponds to the instantaneous generation of multiple secondary events, and thereby violates the assumption of an orderly point process (see Sec. 3.2), we nevertheless consider this simplification to illustrate how the Neyman Type-A counting distribution arises in appropriate limits. This distribution also applies for arbitrary  $h(t)$  in the domain  $T \gg (B - A)$  since all secondary events born of a single primary event, although splayed out over a time  $(B - A)$ , are fully captured within the counting time  $T$  [see Lowen & Teich, 1991, Eq. (21)].

With the help of these results, we plot  $p_Z(n; T)$  in Fig. 10.3 for  $\beta = \frac{1}{2}$  ( $\alpha = 1$ ). Representative results for other parameters appear in Lowen & Teich (1991, Figs. 3–5). The counting distributions displayed in Fig. 10.3 interpolate between the Poisson distribution [Eq. (4.7)] and the Neyman Type-A distribution [Eq. (10.7)], in the short- and long-counting-time limits, respectively.

In fact, the two-parameter Neyman Type-A distribution serves as an excellent approximation for a broad variety of counting distributions associated with shot-noise-driven Poisson processes for arbitrary values of  $T/(B - A)$ . Good agreement over a substantial range of parameters obtains by matching the means and variances of the Neyman Type-A and the exact distributions, as has been explicitly demonstrated for rectangular and exponential impulse response functions (Teich & Saleh, 1987).

Finally, we note that the Neyman Type-A distribution also provides a good approximation for counting distributions associated with the Thomas point process, for these same impulse response functions (Teich & Saleh, 1987). This latter process incorporates the events of the primary homogeneous Poisson process (see Fig. 10.1), along with the secondary events, into the final process. The statistical properties of the Thomas process, which does not belong to the family of doubly stochastic Poisson processes, have been investigated by Matsuo et al. (1983) (see also Secs. 4.5 and 4.6); Thomas (1949) initially developed the exact two-parameter counting distribution that emerges in the limit of large counting times. Various properties and applications of these distributions, as well as doubly stochastic versions thereof, have been studied by Teich (1981).

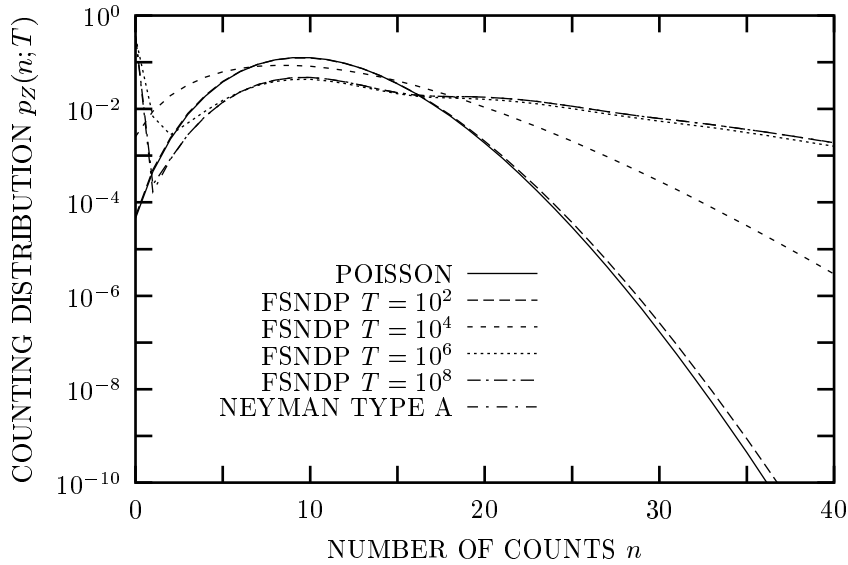


**Fig. 10.3** Counting distribution  $p_Z(n; T)$  vs. number of counts  $n$  for the fractal-shot-noise-driven Poisson process (FSNDP) with  $\beta = \frac{1}{2}$ ,  $A = 1$ ,  $B = 10^5$ ,  $a = 10$ , and  $E[Z] = 10$ . Curves are shown for four values of the counting time:  $T = 10^2, 10^4, 10^6$ , and  $10^8$ . An entire family of counting distributions can be presented while preserving  $E[Z] = 10$  since the fractal-shot-noise-driven Poisson process has five parameters. For small values of the counting time ( $T/A \rightarrow 0$ ), the distribution approaches the Poisson whereas for large values of the counting time ( $T \gg B$ ), it approaches the Neyman Type-A for any  $A$  and  $\beta$ . Since the fractal renewal process depends on only three parameters, it is not possible to provide a similar display in Fig. 7.6.

**10.2.2 Count moments**

Although general expressions for the count moments prove complex, a relatively simple result emerges for the factorial moments. This again takes the form of a recurrence relation (Saleh & Teich, 1982):

$$E\left\{\frac{[Z(t)]!}{[Z(t) - (n + 1)]!}\right\} = \sum_{k=0}^n b_k \binom{n}{k} E\left\{\frac{[Z(t)]!}{[Z(t) - (n - k)]!}\right\}, \quad (10.8)$$

with

$$E\left\{\frac{[Z(t)]!}{[Z(t)]!}\right\} \equiv 1 \quad \text{and} \quad b_k \equiv \mu E\left[\int_{-\infty}^{\infty} [h_T(K, t)]^{k+1} dt\right]. \quad (10.9)$$

Explicit formulas for the particular case of the fractal shot-noise-driven Poisson process exist in this case as well (Lowen & Teich, 1991) (see Sec. A.7.1).



The first factorial moment is the mean number of counts, and rearranging the first two factorial moments yields the variance:

$$\begin{aligned} E[Z(T)] &= E\left\{\frac{[Z(t)]!}{[Z(t) - 1]!}\right\} = b_0 \\ &= \mu E\left[\int_{-\infty}^{\infty} h_T(K, t) dt\right] = \mu T E\left[\int_0^{\infty} h(K, t) dt\right] \\ &= \mu a T; \end{aligned} \tag{10.10}$$

$$\begin{aligned} \text{Var}[Z(T)] &= E\left\{\frac{[Z(t)]!}{[Z(t) - 2]!}\right\} + E[Z(T)] - E^2[Z(T)] \\ &= b_0 + b_1 = \mu a T + \mu E\left\{\int_{-\infty}^{\infty} [h_T(K, t)]^2 dt\right\} \\ &= \mu a T + 2\mu \int_0^T (T - u) \\ &\quad \times E\left[\int_{-\infty}^{\infty} h(K, t) h(K, t + u) dt\right] du. \end{aligned} \tag{10.11}$$

The quantity  $a$  is the expected value of the area of the impulse response function,

$$a \equiv E\left[\int_0^{\infty} h(K, t) dt\right]. \tag{10.12}$$

Equation (9.7) provides that  $E[X] = \mu a$ .

### 10.2.3 Normalized variance

As provided in Sec. 3.4.2, the ratio of the count variance to the count mean yields the normalized variance (Saleh & Teich, 1982):

$$F(T) = 1 + \frac{2}{aT} \int_0^T (T - u) E\left[\int_{-\infty}^{\infty} h(K, t) h(K, t + u) dt\right] du. \tag{10.13}$$

As with any shot-noise-driven Poisson process, this quantity does not depend on the rate  $\mu$  of the driving Poisson process.

Using the impulse response function provided in Eq. (9.2) for fractal shot noise, the normalized variance for the fractal-shot-noise-driven Poisson process becomes (Lowen & Teich, 1991):

$$F(T) = 1 + \frac{2E[K^2]}{aT} \int_0^{\min(T, B-A)} (T - u) \int_A^{B-u} (t^2 + ut)^{-\beta} dt du. \tag{10.14}$$

Equation (10.14) does not in general reduce to a closed-form expression, although closed-form results exist for  $\beta = \frac{1}{2}$  and  $\beta = 2$  (see Sec. A.7.2). In other cases, approximations must suffice.

For  $T \ll A$ , and for any  $B$  and  $\beta$ , the normalized variance varies linearly with  $T$  (Lowen & Teich, 1991),

$$F(T) \approx 1 + \frac{E[K^2]}{a} \left[ \int_A^B t^{-2\beta} dt \right] T = 1 + \frac{\text{Var}[X]}{E[X]} T, \quad (10.15)$$

as shown in Sec. A.7.2.

In the range  $A \ll T \ll B$ ,  $F(T)$  approaches a number of simple forms (Lowen & Teich, 1991) that depend on  $\beta$  (see Sec. A.7.2):

$$F(T) \approx 1 + \frac{E[K^2]}{E[K]} \times \begin{cases} \frac{1-\beta}{1-2\beta} B^{-\beta} T & 0 \leq \beta < \frac{1}{2} \\ \frac{1}{2} B^{-1/2} \ln(B/T) T & \beta = \frac{1}{2} \\ \frac{\Gamma(\alpha/2) \Gamma(1-\alpha)}{(1+\alpha) \Gamma(1-\alpha/2)} B^{-\alpha/2} T^\alpha & \frac{1}{2} < \beta < 1 \\ & (1 > \alpha > 0) \\ \frac{\ln^2(T/A)}{\ln(B/A)} & \beta = 1 \\ (\beta-1)^{-1} A^{1-\beta} & \beta > 1. \end{cases} \quad (10.16)$$

In the domain  $\frac{1}{2} < \beta < 1$ , we cast the expression in terms of  $\alpha \equiv 2(1-\beta)$ , rather than in terms of  $\beta$ , to highlight the scaling behavior of this measure over this range of exponents ( $0 < \alpha < 1$ ).

Finally, for  $T \gg B$ , and for any  $A$  and  $\beta$ , the normalized variance approaches a constant value (see Sec. A.7.2; Lowen & Teich, 1991) given by

$$F(T) \approx 1 + \frac{E[K^2]}{E^2[K]} a. \quad (10.17)$$

For a deterministic impulse response function, this reduces to  $F(T) \approx 1 + a$ . This result for  $T \gg B$  is consistent with the Neyman Type-A counting distribution set forth in Eq. (10.7), as required for any shot-noise-driven Poisson process (Saleh & Teich, 1982).

We plot the normalized variance  $F(T)$  in Fig. 10.4 for a range of power-law exponents  $\beta$ , as a function of the counting time  $T$ .

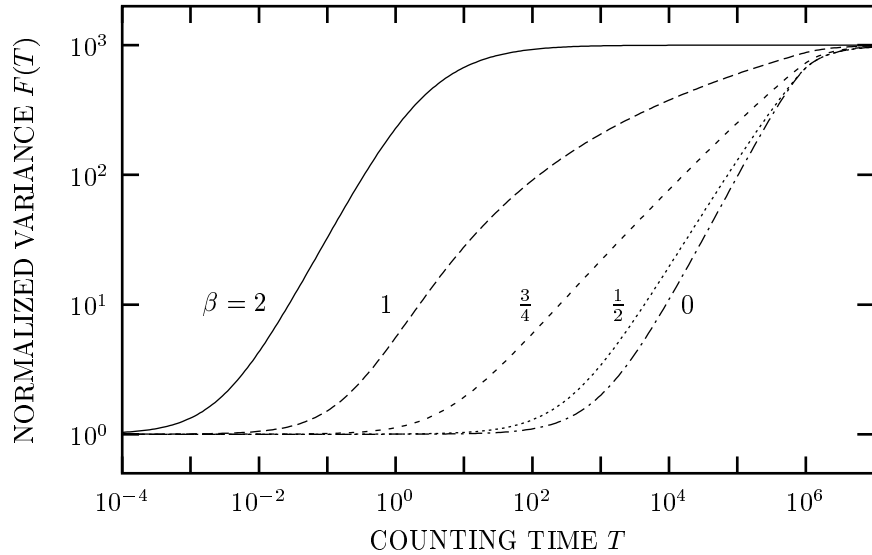


**Fig. 10.4** Normalized variance  $F(T)$  vs. counting time  $T$  provided in Eq. (10.14) for five values of the power-law exponent  $\beta$ : 0,  $\frac{1}{2}$ ,  $\frac{3}{4}$ , 1, and 2. The remaining parameters are fixed at  $A = 1$ ,  $B = 10^6$ , and  $a = 10^3$  ( $K$  is chosen to be deterministic). For  $\frac{1}{2} < \beta < 1$ , the normalized variance grows as  $T^{2-2\beta} = T^\alpha$ , in accordance with Eq. (10.16).

**10.2.4 Normalized Haar-wavelet variance**

We calculate the normalized Haar-wavelet variance  $A(T)$  set forth in Sec. 3.4.3 by using Eq. (10.14) in conjunction with Eq. (3.41). The calculations depend on the value of  $T$ , and three domains emerge:  $T \leq (B - A)/2$ ,  $(B - A)/2 < T \leq (B - A)$ , and  $T > (B - A)$ . Rather than using Eq. (10.14), we could alternatively insert Eqs. (10.15)–(10.17) for  $F(T)$  directly into Eq. (3.41) to provide a parallel set of equations for  $A(T)$ .

Effecting such a direct substitution requires caution, however, as discussed at the end of Sec. 5.2.4. As shown by Eqs. (5.37)–(5.39), the use of asymptotic formulas for  $F(T)$  in Eq. (3.41) yields invalid results when linear terms dominate  $F(T) - 1$ . This caution specifically applies to Eq. (10.15) for all values of  $\beta$  and to Eq. (10.16) for  $\beta < \frac{1}{2}$ . For substitution into Eq. (3.41) we must therefore either use Eq. (10.14) directly, or employ versions of Eqs. (10.15)–(10.17) that retain higher-order terms.

Using these methods, we carry out calculations in Sec. A.7.3 that lead to the following results for the normalized Haar-wavelet variance.

For  $T \ll A$ , the dependence of  $A(T)$  on  $T$  is quadratic:

$$A(T) \approx 1 + (3a)^{-1} E[K^2] (A^{-2\beta} + B^{-2\beta}) T^2. \tag{10.18}$$

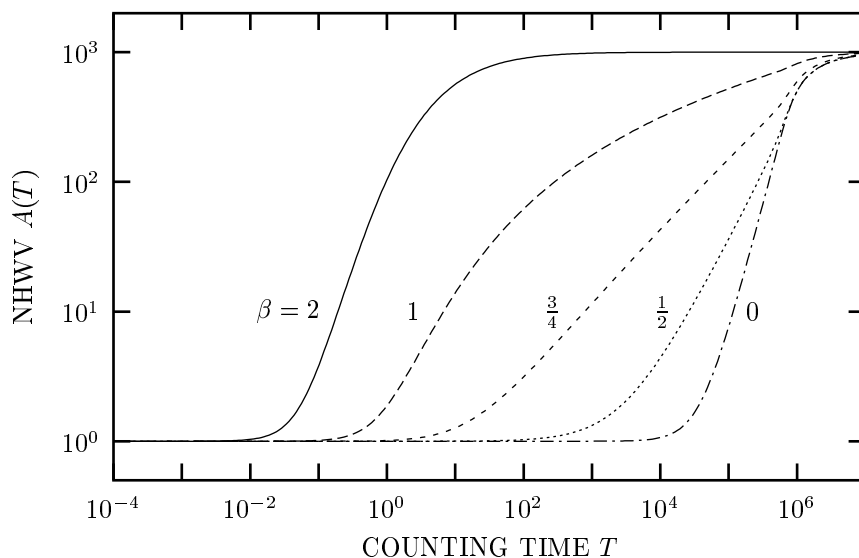


**Fig. 10.5** Normalized Haar-wavelet variance  $A(T)$  vs. counting time  $T$  derived via Eqs. (10.14) and (3.41) for five values of the power-law exponent  $\beta$ : 0,  $\frac{1}{2}$ ,  $\frac{3}{4}$ , 1, and 2. The remaining parameters are fixed at  $A = 1$ ,  $B = 10^6$ , and  $a = 10^3$  ( $K$  is chosen to be deterministic). For  $0 < \beta < 1$ , the normalized Haar-wavelet variance grows as  $T^{2-2\beta} = T^\alpha$ , in accordance with Eq. (10.19).

In the range  $A \ll T \ll B$ ,  $A(T)$  approaches a simple form that depends on  $\beta$  (see Sec. A.7.3):

$$A(T) \approx 1 + \frac{E[K^2]}{E[K]} \times \begin{cases} \frac{(2^\alpha - 2) \Gamma(\alpha/2) \Gamma(2 - \alpha)}{(\alpha^2 - 1) \Gamma(1 - \alpha/2)} B^{-\alpha/2} T^\alpha & \begin{matrix} 0 < \beta < \frac{1}{2} \\ (2 > \alpha > 1) \end{matrix} \\ \ln(2) B^{-1/2} T & \begin{matrix} \beta = \frac{1}{2} \\ (\alpha = 1) \end{matrix} \\ \frac{(2 - 2^\alpha) \Gamma(\alpha/2) \Gamma(2 - \alpha)}{(1 - \alpha^2) \Gamma(1 - \alpha/2)} B^{-\alpha/2} T^\alpha & \begin{matrix} \frac{1}{2} < \beta < 1 \\ (1 > \alpha > 0) \end{matrix} \\ \frac{\ln^2(T/A)}{\ln(B/A)} & \beta = 1 \\ (\beta - 1)^{-1} A^{1-\beta} & \beta > 1. \end{cases} \quad (10.19)$$

We have cast some of these expressions in terms of  $\alpha \equiv 2(1 - \beta)$ , rather than in terms of  $\beta$ , to highlight the scaling behavior of  $A(T)$ . Scaling extends over the range  $0 < \beta < 1$  ( $0 < \alpha < 2$ ). This range exceeds that over which scaling extends for the

normalized variance  $F(T)$  inasmuch as the latter cannot increase faster than  $T^1$ , as discussed in Sec. 5.2.3:  $\frac{1}{2} < \beta < 1$  ( $1 > \alpha > 0$ ).

Finally, for  $T \gg B$ , and for any  $A$  and  $\beta$ , Eqs. (3.41) and (10.17) provide that  $A(T) = 2F(T) - F(2T) = F(T)$  so that  $A(T)$  is constant. This is, of course, the domain in which the Neyman Type-A counting distribution prevails.

The normalized Haar-wavelet variance  $A(T)$  is displayed in Fig. 10.5 for a range of power-law exponents  $\beta$ , as a function of the counting time  $T$ .

### 10.3 TIME STATISTICS

The probability densities for the forward recurrence time,  $p_\theta(t)$ , and the interevent time,  $p_\tau(t)$ , are determined from the probability that zero events occur in an interval of duration  $T$ ,  $p_Z(0; T)$ , as its first two derivatives (see Secs. 3.3.1 and 3.4.1). Combining Eqs. (3.30) and (10.3) provides

$$p_\tau(t) = \frac{1}{E[X]} \frac{d^2}{dt^2} \exp\left(\mu E\left[\int_{-\infty}^{\infty} \{\exp[-h_t(K, u)] - 1\} du\right]\right), \quad (10.20)$$

where  $X(t)$  represents the shot-noise process that emerges at the output of the linear filter (see Fig. 10.1).

Section A.7.4 provides detailed expressions for  $p_\theta(t)$  and  $p_\tau(t)$  for a deterministic impulse response function. With the help of these results, we plot the interevent-interval probability density function  $p_\tau(t)$  in Fig. 10.6 for several values of the power-law exponent  $\beta$ . Representative results for other parameters, and for the forward-recurrence-time density, are presented in Lowen & Teich (1991, Figs. 9–12).

The significant differences among the curves in Fig. 10.6 reflect the varying degree of clustering that fractal-shot-noise-driven Poisson processes can exhibit. A large degree of clustering is accompanied by an increase in the probability of very short and very long interevent times, at the expense of times near the mean, relative to an exponential density of the same mean. Figure 10.6 shows that the clustering increases as  $\beta$  increases. To explain this, we observe that the clustering has its origin in the variations of the fractal shot-noise rate  $X(t)$ . For larger values of  $\beta$ , particularly  $\beta > 1$ , the majority of the area of the impulse response function lies in a small region near the onset time  $A$ , with proportionately less area in the tail. For smaller values of  $\beta$ , in contrast, the value of the impulse response function changes far less over its duration  $B - A$ . Thus, the fractal shot-noise rate  $X(t)$  exhibits greater variations for large values of  $\beta$ , and the fractal-shot-noise-driven Poisson process therefore concomitantly exhibits more clustering, assuming that all other parameters remain constant.

For  $\tau = 0$  and all values of  $\beta$  we have (Lowen & Teich, 1991)

$$p_\tau(0) = 1/E[\tau] + E[\tau] \text{Var}[X], \quad (10.21)$$

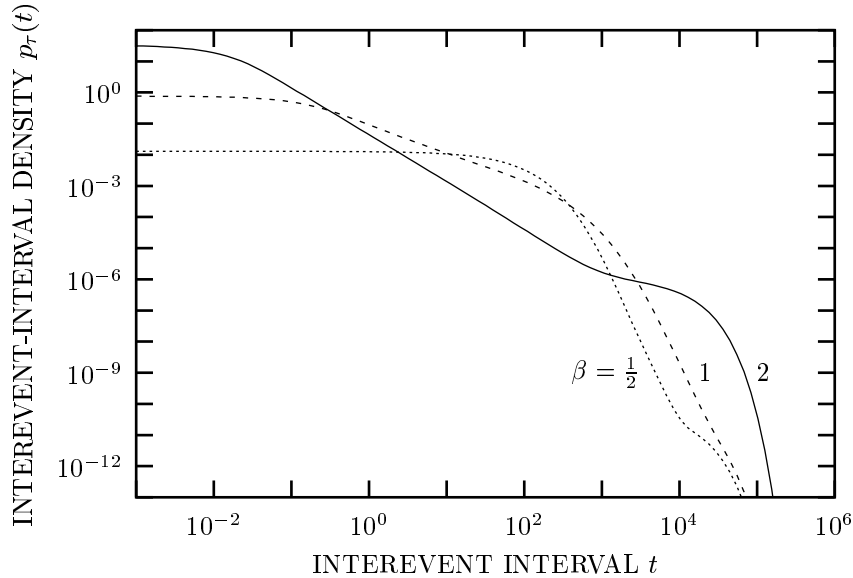


**Fig. 10.6** Interevent-interval probability density function,  $p_\tau(t)$  vs.  $t$ , for the fractal-shot-noise-driven Poisson process. We display results for three values of the power-law exponent:  $\beta = \frac{1}{2}$ , 1, and 2. The remaining parameters are fixed at  $A = 1$ ,  $B = 10^5$ ,  $a = 100$ ,  $\mu = 10^{-4}$ , and  $E[\tau] = 100$  ( $K$  is chosen to be deterministic). The probability density exhibits a range of power-law behaviors as the time  $t$  and the power-law exponent  $\beta$  vary.

whereas in the limit  $\tau \rightarrow \infty$  the probability density function approaches exponential form (Lowen & Teich, 1991),

$$p_\tau(t) \rightarrow \frac{\mu(1 - e^{-a})^2}{a} \exp[-\mu t(1 - e^{-a})], \tag{10.22}$$

by virtue of Eqs. (3.30) and (10.6). The exponential nature of the primary Poisson process  $dN_1(t)$  carries over to the interevent-interval statistics for large interevent times  $\tau$ . For  $\beta > 1$ , the concentration of the area  $a$  of the impulse response function near the onset time  $A$  results in tight clustering of the events of  $dN_2(t)$  following primary events. The long intervals thus essentially derive from the primary process  $dN_1(t)$ , and  $p_\tau(t)$  exhibits an exponential tail, albeit with reduced amplitude in comparison with a homogeneous Poisson process. Even for  $\beta < 1$ , interevent intervals longer than  $B - A$  usually derive from the primary process, particularly for small values of  $\mu(B - A)$ , where  $X(t) = 0$  for significant periods of time. This, too, results in an exponential tail.

10.4 COINCIDENCE RATE

The coincidence rate  $G(t)$  for a doubly stochastic Poisson process closely follows the autocorrelation of its driving rate, as provided by Eq. (4.24). Since the fractal-shot-noise-driven Poisson process belongs to the family of doubly stochastic Poisson processes, this equation applies here.

Inserting Eq. (9.20) for the autocorrelation of the  $X(t)$  into Eq. (4.24) provides an expression for the coincidence rate:

$$G(t) = E[X] \delta(t) + E^2[X] + \begin{cases} \mu E[K^2] \int_A^{B-|t|} (u^2 + |t|u)^{-\beta} du & |t| < B - A \\ 0 & |t| \geq B - A. \end{cases} \quad (10.23)$$

Closed-form expressions for  $G(t)$  exist for  $\beta = \frac{1}{2}, 1$  and  $2$  (Lowen & Teich, 1991).

When the delay time  $t$  is small,  $G(t)$  approaches a constant value for any power-law exponent  $\beta$ :

$$G(t) = E^2[X] + \mu E[K^2] \int_A^B t^{-2\beta} dt. \quad (10.24)$$

In the region  $A \ll |\tau| \ll B$ , the coincidence rate takes a variety of forms for different values of  $\beta$  (Lowen & Teich, 1991, Appendix G):

$$G(t) = E^2[X] + \mu E[K^2] \times \begin{cases} \frac{(1-\beta)^2}{(1-2\beta)} B^{-1} & 0 \leq \beta < \frac{1}{2} \\ \frac{1}{4} B^{-1} \ln(B/|t|) & \beta = \frac{1}{2} \\ \frac{\alpha \Gamma(1+\alpha/2) \Gamma(1-\alpha)}{2\Gamma(1-\alpha/2)} B^{-\alpha} |t|^{\alpha-1} & \frac{1}{2} < \beta < 1 \\ \frac{\ln(|t|/A)}{\ln^2(B/A)} |t|^{-1} & \beta = 1 \\ (\beta - 1) A^{\beta-1} |t|^{-\beta} & \beta > 1. \end{cases} \quad (10.25)$$

In the domain  $\frac{1}{2} < \beta < 1$ , we express the results in terms of  $\alpha \equiv 2(1 - \beta)$  rather than in terms of  $\beta$ , again to emphasize the scaling behavior of this measure.

The coincidence rate  $G(t)$ , as a function of the delay time  $t$ , appears in Fig. 10.7. To avoid the constant term  $E^2[X]$  from obscuring the variation in  $G(t)$ , we actually graph the expression  $G(t) - E^2[X]$  rather than  $G(t)$  itself.

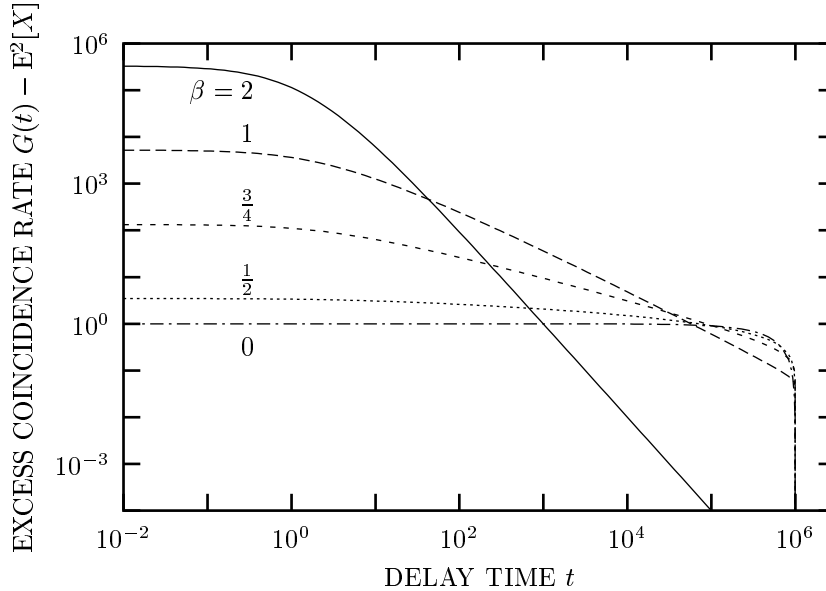


**Fig. 10.7** Excess coincidence rate,  $G(t) - E^2[X]$  vs. delay time  $t$ , obtained from Eq. (10.23) for five values of the power-law exponent:  $\beta = 0, \frac{1}{2}, \frac{3}{4}, 1,$  and  $2$ . The remaining parameters are set at fixed values for all curves:  $A = 1, B = 10^6, \mu = 1,$  and  $a = 10^3$  ( $K$  is chosen to be deterministic). In accordance with Eq. (10.25), the functions corresponding to  $\beta > \frac{1}{2}$  exhibit approximate power-law behavior, with various exponents, over a good portion of their range. Note the abrupt drop near  $t = B - A \approx 10^6$ , where  $G(t) - E^2[X] \rightarrow 0$  in accordance with Eq. (10.23).

**10.5 SPECTRUM**

We turn now to the spectrum of the fractal-shot-noise-driven Poisson process. In accordance with Eq. (4.25), the spectrum of  $dN_2(t)$  differs from that of  $X(t)$  only by an additive constant term,  $E[X]$ . In the domain  $\beta < 1$  and  $A \ll B < \infty$ , where  $S_X(f)$  behaves as  $1/f$ -type noise (see Table 9.1), we insert Eq. (9.30) in Eq. (4.25) to obtain

$$S_{N_2}(f) = S_X(f) + E[X] \approx \mu E[K^2] \Gamma^2(\alpha/2) (2\pi f)^{-\alpha} + (2/\alpha)\mu E[K] B^{\alpha/2}, \quad (10.26)$$

where we have employed the approximation  $A \rightarrow 0$ , valid for  $A \ll B$  and  $\beta < 1$ .

Figure 10.8 illustrates the spectrum for the fractal-shot-noise-driven Poisson process using the same impulse response functions (abrupt cutoff and exponential), and the same parameters, as those used to generate the fractal-shot-noise spectrum displayed in Fig. 9.4. We can define a crossover frequency by equating the two terms



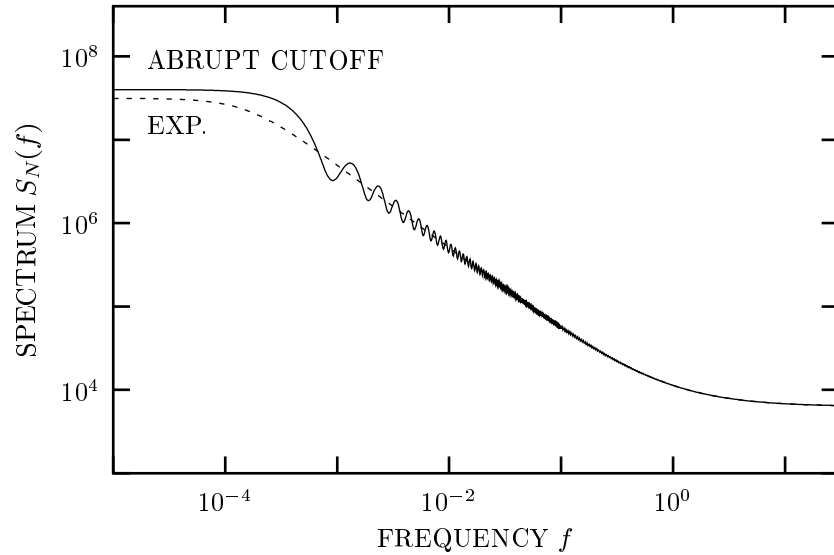


**Fig. 10.8** Spectrum  $S_N(f)$  vs. frequency  $f$  for the fractal-shot-noise-driven Poisson process. The parameter values are the same as those used to generate the curves for the fractal-shot-noise spectrum,  $S_X(f)$ , displayed in Fig. 9.4:  $\beta = \frac{1}{2}$  ( $\alpha = 1$ ),  $A = 0$ ,  $B = 1\,000$ ,  $K = 100$ , and  $\mu = 1$ . For sufficiently high frequencies, the spectrum exhibits  $1/f^\alpha$  behavior, with  $\alpha = 1$ . The impulse response function with an abrupt cutoff in the time domain results in oscillations in the frequency domain, whereas an exponential transition yields a smooth curve. In the high-frequency limit, both curves approach the asymptotic value,  $\lim_{f \rightarrow \infty} S_N(f) = E[X] = 2\,000\sqrt{10} \doteq 6325$ .

on the right-hand side of Eq. (10.26):

$$\begin{aligned} \mu E[K^2] \Gamma^2(\alpha/2) (2\pi f_S)^{-\alpha} &= (2/\alpha) \mu E[K] B^{\alpha/2} \\ \alpha \Gamma^2(\alpha/2)/2 &= (E[K]/E[K^2]) (2\pi f_S)^\alpha B^{\alpha/2}. \end{aligned} \quad (10.27)$$

## 10.6 RELATED POINT PROCESSES

### 10.6.1 Point process in the Gaussian limit of fractal shot noise

Under suitable conditions, the probability density of the driving fractal-shot-noise rate  $X(t)$  converges to a Gaussian form [see Eqs. (9.11) and (9.12), as well as Table 9.1], and indeed  $X(t)$  becomes a Gaussian process. As provided by the central limit theorem, this takes place in the limit  $\mu \rightarrow \infty$  if  $E[K^k] < \infty$  for all  $k$ ,  $A > 0$ , and  $B < \infty$  for  $\beta \leq 1$  (Lowen & Teich, 1990). Over this range of  $\beta$ , the spectrum

varies as  $1/f^{2-2\beta} = 1/f^\alpha$ , and  $X(t)$  converges to a **fractal Gaussian process** (see Sec. 6.3.3). The resulting point process  $dN_2(t)$  then becomes a **fractal-Gaussian-process-driven Poisson process** (see Fig. 5.5, Secs. 6.3.3 and 8.4, and Chapter 12).

### 10.6.2 Fractal-shot-noise-driven integrate-and-reset point process

The discussion thus far has centered on point processes produced by fractal shot noise driving a Poisson generator. However, fractal shot noise can also serve as the rate function for other generation mechanisms, such as the integrate-and-reset point process set forth in Sec. 4.4 (Turner et al., 1997). The **fractal-shot-noise-driven integrate-and-reset process**, as an example, suitably characterizes spontaneous action-potential generation in the visual system (Teich & Lowen, 2003).

Many of the properties of the fractal-shot-noise-driven integrate-and-reset process readily derive from the results set forth in Sec. 4.4, together with the results obtained earlier in this chapter and in Chapter 9. In particular, the statistics over time scales that are substantially longer than  $E[\tau]$  (corresponding to frequencies much lower than  $1/E[\tau]$ ) virtually coincide with those of the fractal-shot-noise-driven Poisson process. This conclusion follows because Poisson processes introduce few fluctuations over these time scales, while integrate-and-reset processes introduce none.

The statistics that are manifested over times comparable to, or less than,  $E[\tau]$  depend largely on the amplitude distribution of the fractal shot noise; Sec. 9.2 and Eqs. (4.37) and (4.38) prove useful for these calculations. Over all time scales, fractal shot noise itself provides useful results for the second-order statistics of the fractal-shot-noise-driven integrate-and-reset process, through Eq. (4.36).

### 10.6.3 Hawkes point process

We now consider the nontrivial, critical, self-exciting point process displayed in Fig. 10.9. A classical **Hawkes point process** (Hawkes, 1971) comprises a Poisson process whose output drives a linear filter  $h(t)$  to produce a continuous stochastic process  $X(t)$ . The sum of this process and an external input (a constant  $\mu_0$  in the example at hand) forms a function  $\mu(t)$  that serves as the rate for the original Poisson process. The stochastic process  $X(t)$  therefore shares some similarity with shot noise. Because the resulting point process  $dN(t)$  modulates itself in a feedback loop, it is a special **self-exciting point process**.

In order that the process be stationary, the area of the impulse response function  $h(t)$  must lie below unity; were that not the case, the rate would grow exponentially over time. The external input  $\mu_0$  can, instead, be a time-varying function that integrates to a finite value. It is then possible to have an impulse response function with unity area, but it turns out that the ensuing process has trivial characteristics for general forms of  $h(t)$ . However, the selection of fractal forms for  $h(t)$  (more precisely, those with heavy tails) results in nontrivial critical Hawkes point processes, which themselves have fractal properties (Brémaud & Massoulié, 2001).

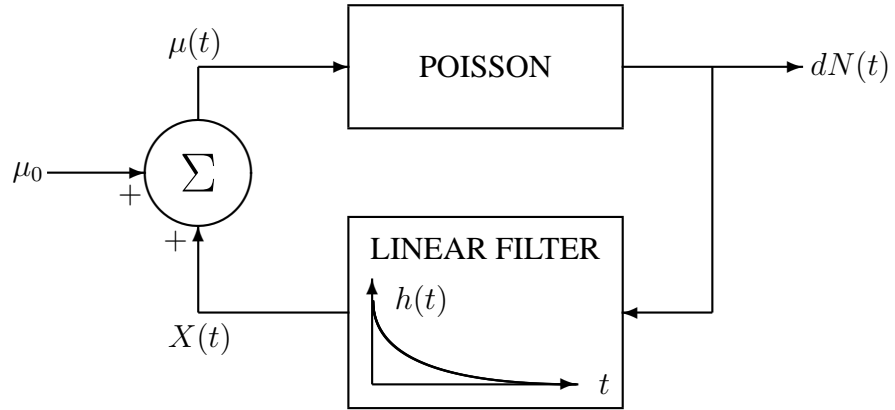


**Fig. 10.9** A stochastic rate process  $\mu(t)$  modulates the rate of a Poisson process, yielding a classical Hawkes point process  $dN(t)$ . This point process serves as the input to a linear filter with impulse response function  $h(t)$ . A continuous-time stochastic process  $X(t)$ , which is a form of generalized shot noise, emerges from the output of this filter. The sum of  $X(t)$  and an external constant rate  $\mu_0$  provides the stochastic rate process  $\mu(t)$ , completing the loop.

**10.6.4 Bartlett–Lewis fractal point process**

We conclude this chapter by examining a process constructed from nonfractal renewal processes to which fractal behavior is imparted in a different way. Consider a Bartlett–Lewis-type cascaded point process (see Sec. 4.5) constructed from a primary Poisson point process  $dN_1(t)$ , each event of which initiates a segment of a secondary Poisson point process  $dN_{2,k}(t)$  which, in turn, terminates after a certain number of secondary events  $M_k$ . The superposition of all secondary events forms the final point process  $dN_3(t)$ . Primary events (illustrated as dashed vertical lines in the secondary processes in Fig. 4.2) can be excluded or included in the final process. A number of variations on this theme have appeared in the literature (Grüneis, 1984; Grüneis & Baiter, 1986; Grüneis & Musha, 1986; Grüneis, 1987, 2001). This model finds application in characterizing computer network traffic, as discussed in Secs. 13.5.4 and 13.6.

Fractal behavior in this process arises from the imposition of a power-law distribution on the number of events  $M_k$  associated with each secondary process  $dN_{2,k}(t)$  before its termination. Specifically, let this number follow the distribution

$$\Pr\{M_k = m\} = m^z / \sum_{l=1}^{M_{\max}} l^z, \tag{10.28}$$

where  $M_k$  ranges from a minimum of one event to a maximum of  $M_{\max}$  events. A single segment of a Poisson process of mean interevent interval  $E[\tau_2]$ , and of fixed, deterministic duration with  $M_k$  events, has a spectrum given by (Grüneis & Musha, 1986)

$$2(2\pi f E[\tau_2])^{-2} \{ \text{Re}[(1 + i2\pi f E[\tau_2])^{1-M_k}] - 1 \}. \tag{10.29}$$

If  $M_k$  now becomes a random variable taking values with probabilities given by Eq. (10.28), and if each event in the primary process  $dN_1(t)$ , with mean interevent interval  $E[\tau_1]$ , initiates such a secondary process, the resulting cascaded process  $dN_3(t)$  exhibits a spectrum of the form

$$S_{N_3}(f) = (E[M_k]/E[\tau_1])^2 \delta(f) + E[M_k]/E[\tau_1] + \frac{2 \sum_{l=1}^{M_{\max}} l^z \{ \text{Re}[(1 + i2\pi f E[\tau_2])^{1-l}] - 1 \}}{E[\tau_1] (2\pi f E[\tau_2])^2 \sum_{l=1}^{M_{\max}} l^z}. \quad (10.30)$$

The mean interevent interval of the secondary processes,  $E[\tau_2]$ , and the mean duration of the secondary processes,  $E[\tau_2] E[M_k]$ , then play the roles of the cutoffs  $A$  and  $B$  associated with the impulse response function  $h(t)$  of the fractal-shot-noise-driven Poisson process. The spectrum remains relatively constant for frequencies outside the reciprocals of these two times. However, for frequencies well within these limits, scaling behavior emerges for certain values of the event-number distribution exponent  $z$  (Grüneis & Musha, 1986). The spectrum then turns out to follow the form

$$\alpha = \begin{cases} 0 & z \leq -3 \\ z + 3 & -3 < z < -1 \\ 2 & -1 \leq z. \end{cases} \quad (10.31)$$

This relationship indicates that the process at hand generates  $1/f^\alpha$  noise over the extended range  $0 < \alpha < 2$ .

Both the fractal Bartlett–Lewis cascaded process and the fractal Neyman–Scott cluster process are plausible models for describing computer network traffic, as discussed extensively in Chapter 13.

**Problems**

**10.1 Interevent-interval density function for large intervals** Equation (10.22) shows that the interevent-interval probability density decays as an exponential for large interevent intervals  $\tau$ . Show heuristically that this holds for the simple case  $\tau > B - A$ .

**10.2 Normalized variance for rectangular impulse response functions** Evaluate Eq. (10.14) explicitly for the case  $\beta = 0$ , where the impulse response functions reduce to rectangles. Find the limit of the resulting expression when  $A \ll T \ll B$ , and show that this limit agrees with Eq. (10.16).

**10.3 Interval density function associated with a single impulse response** Figure 10.6 displays a set of interevent-interval probability densities  $p_\tau(t)$  for several values of the parameter  $\beta$ . For the particular curve associated with  $\beta = 2$ , the density  $p_\tau(t)$  decays as a power-law function of the interval. Consider a single impulse

response function, and show that the density  $p_\tau(t)$  of the resulting process indeed follows this power-law form. Find the slope and extent of this scaling region. Show that this behavior holds for general  $\beta > 1$ .

**10.4** *Designing a fractal-shot-noise-driven Poisson process* By appropriate selection of the parameters  $\beta$ ,  $A$ ,  $B$ ,  $\mu$ , and  $K$ , we can design a fractal-shot-noise-driven Poisson process that exhibits a  $1/f^\alpha$  spectrum, a cutoff frequency  $f_S$ , and a rate of events with a particular mean value.

**10.4.1.** Identify the appropriate equations in the text that relate these three design values to the five parameters of the fractal-shot-noise-driven Poisson process.

**10.4.2.** Suppose we also choose values for the coefficient of variation and skewness of the rate, for example, in an attempt to fully specify the process. Using the specific case  $\alpha = 1$ ;  $f_S = 1$ ; an average rate of unity; and fixed, deterministic  $K$  as an example, discuss the constraints on the five design values. One might wish to employ a rate with a large coefficient of variation to yield an appreciable amount of fluctuation in the numbers of events generated in  $dN_2(t)$ , and also a small skewness to better approximate a fractal Gaussian process. Show that attempting to simultaneously specify both large values of the rate coefficient of variation and small values of the rate skewness leads to conflicting requirements and unspecified parameters.

**10.4.3.** Rather than specifying higher moments of the rate, we instead seek to use the following two constraints:  $B/A = 10^3$  for an appreciable range of frequencies following the  $1/f$  spectrum, and  $A = 1/f_S$  to ensure that the spectrum indeed follows this form up to  $f = f_S$ . Design a fractal-shot-noise-driven Poisson process with the specific values given here and in Prob. 10.4.2, and find the coefficient of variation and the skewness of the rate.

**10.5** *Impulse response functions without cutoffs* Impulse response functions without cutoffs lead to fractal-shot-noise processes with infinite moments (see Chapter 9). Suppose that we nevertheless employ such a shot-noise-process as a rate for a Poisson process, generating a point-process output  $dN_2(t)$ . Describe this point process, and comment on its orderliness.

**10.6** *Photon statistics of Čerenkov radiation* Charged particles traveling faster than the group velocity of light in a transparent medium emit photons, often in the visible range. Čerenkov was the first to systematically examine this phenomenon in a series of experiments conducted during the years 1934–1938 (see, for example, Čerenkov, 1934, 1937, 1938).

One can use electromagnetic theory to show that the fractal-shot-noise-driven Poisson process provides a useful model for describing the light produced by Čerenkov radiation arising from a sparse random stream of charged particles. Consider a charged particle traveling along the positive  $x$ -axis through a transparent, non-ferromagnetic medium of refractive index  $n$ , at a speed  $v > c/n$  where  $c$  is the speed of light in free space, as shown in Fig. 10.10. We define the quantity  $J \equiv [(nv/c)^2 - 1]^{1/2}$ ; it is a function of the degree to which the particle velocity exceeds the Čerenkov limit  $c/n$ . We calculate the electric and magnetic fields at a distance  $d$  from the  $x$ -axis, where we choose the arbitrary point in the  $x$ - $z$  plane  $\{-Jd, 0, d\}$  for algebraic

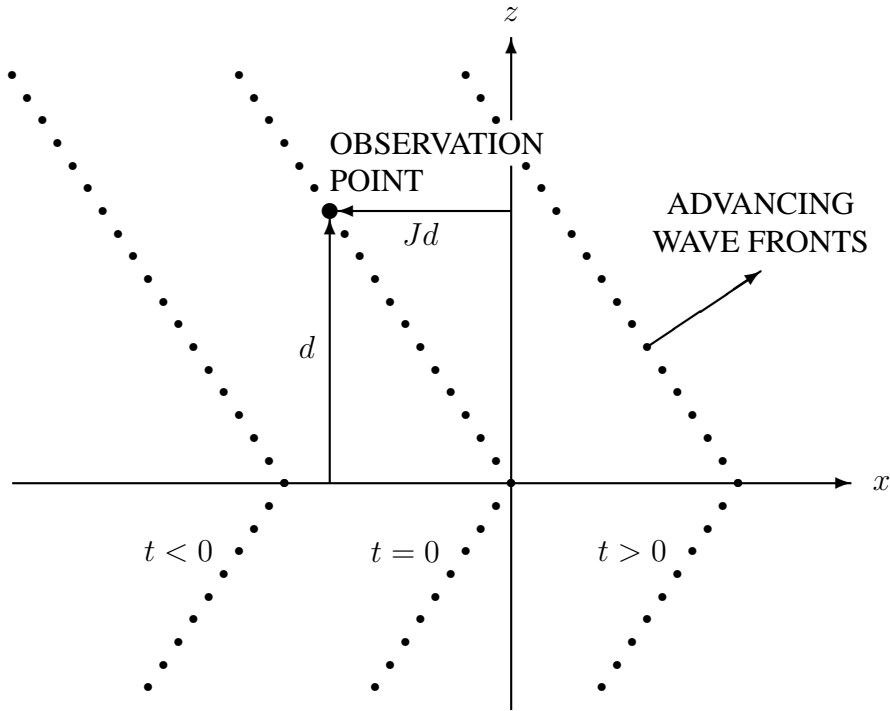


**Fig. 10.10** A charged particle moving faster than the speed of light in a medium emits Čerenkov radiation. At the point  $\{-Jd, 0, d\}$ , the photon flux density decays as an inverse power-law function of time. We illustrate three wavefronts for a particle traveling along the  $x$ -axis, corresponding to times  $t < 0$ ,  $t = 0$ , and  $t > 0$ . The particle passes the origin at  $t = 0$ .

simplicity. We assume that the particle does not experience substantial deceleration while significantly close to this observation point. In accordance with the Frank–Tamm theory (see Jelley, 1958; Zrelov, 1968), we obtain scalar and vector potentials that satisfy the Lorentz gauge condition

$$\phi_L = 2qn^{-2} [(x - vt)^2 - J^2(y^2 + z^2)]^{-1/2} \quad (10.32)$$

$$\mathbf{A}_L = n^2c^{-1} \mathbf{v} \phi_L, \quad (10.33)$$

respectively, where  $q$  represents the charge of the particle.

The corresponding electric and magnetic fields associated with this single charged particle traveling through the medium are written in terms of the scalar and vector potentials as

$$\mathbf{E} = -\nabla\phi_L - c^{-1}\partial\mathbf{A}_L/\partial t \quad (10.34)$$

and

$$\mathbf{H} = \mathbf{B} = \nabla \otimes \mathbf{A}_L, \quad (10.35)$$

where  $\otimes$  denotes the vector cross product. The Poynting vector,

$$\mathbf{S} \equiv (4\pi)^{-1} c \mathbf{E} \otimes \mathbf{H}, \quad (10.36)$$

characterizes the energy flux density (intensity) and its direction; its magnitude specifies only the energy flux density.

The spectrum of the light may be calculated by Fourier-transform methods (see Jelley, 1958; Zrelow, 1968), or via Eqs. (9.28) and (4.25). We denote  $E[\nu]$  as the mean frequency of the light, so that the mean photon energy is  $hE[\nu]$ , where  $h$  is Planck's constant. This permits us to convert the time-varying intensity generated by a single traveling charged particle into an approximate expression for the time-varying photon flux density generated by the particle (see Saleh & Teich, 1991, Chaps. 5 and 11):

$$h(t) \approx |\mathbf{S}| / hE[\nu]. \quad (10.37)$$

**10.6.1.** Over what range of times does the foregoing description apply?

**10.6.2.** Derive  $h(t)$  as defined in Eq. (10.37), and cast it in the form of a simple power-law impulse-response function as in Eq. (9.2), assuming that the refractive index of the medium departs significantly from unity. Obtain power-law exponents and cutoff values in terms of quantities previously given, and give an approximate form with a single power-law exponent.

**10.6.3.** What changes if the index of refraction differs only slightly from unity?

**10.6.4.** Under what conditions does a stream of charged particles yield a sequence of photons well described by the fractal-shot-noise-driven Poisson process?

**10.7 Earthquake occurrences** A full description of earthquake activity requires a marked spatiotemporal point process, so that the time and location of the epicenters, as well as the total energy dissipated, is specified for each seismic event. The analysis of earthquake patterns reveals that earthquakes obey power-law statistics in their magnitude distributions, in their spatial clustering, and in their second-order time statistics (see, for example, Kagan & Knopoff, 1987; Lapenna et al., 1998; Telesca et al., 1999; Telesca, Cuomo, Lapenna & Macchiato, 2002b, which provides a recent overview). However, in keeping with the approach used throughout this book, we pay no heed to the spatial and energy information; rather, we treat all seismic activity within a specified area, and above a limiting energy, as the events of an unmarked point process.

The statistician David Vere-Jones (1970) used a version of the fractal-shot-noise-driven Poisson process to model shallow ( $< 100$  km) earthquakes of magnitude  $> 4.5$  that occurred between January 1942 and September 1961 in New Zealand.<sup>3</sup> He obtained good fits to both the mean rate of earthquakes (about 22 per year), and the variance–time curve, over a range of 0.1 to 1.5 years. From the latter statistic at 0.1 year, and from the count-based autocorrelation  $R_Z(1, 0.1 \text{ year})$ , he concluded

<sup>3</sup> An often-used alternative model for earthquake occurrences is self-organized criticality (see Sec. 2.7.6); however, recent results indicate that earthquake data are not in good accord with this theory (Yang, Du & Ma, 2004).

that the average cluster contained six earthquakes and that the expected number of earthquakes remaining in a cluster decayed with time as  $t^{-1/4}$ . He further obtained a cluster start time of 2.3 days after a primary event, and assumed that no mechanism terminated the clusters at any specific time after that.

**10.7.1.** From the information provided above, identify the fractal-shot-noise-driven Poisson process employed by Vere-Jones in terms of the parameters used in this chapter.

**10.7.2.** The value of  $\beta$  used in the model (which is close to but greater than unity), together with  $B = \infty$ , leads to a long tail in the seismic activity. How much time must pass after a cluster starts so that, with 0.8 probability, no events still remain in the cluster?

**10.8 Diffusion** Consider a collection  $u_0$  of infinitesimal particles, all initially at some point  $\mathbf{x}_0$  of a Euclidean space of (integer) dimension  $D_E < 4$  at a starting time  $t = 0$ . The concentration  $u$  at some other point  $\mathbf{x}$  and some later time  $t$  will then vary in proportion to a Gaussian density with a variance that increases with time in a power-law fashion (see, for example, Pinsky, 1984),

$$u(\mathbf{x}, t) = u_0 (4\pi\Delta t)^{-D_E/2} \exp\left(-\frac{|\mathbf{x} - \mathbf{x}_0|^2}{4\Delta t}\right), \quad (10.38)$$

where  $\Delta$  is the diffusion constant. We assume that the particles have some lifetime  $t_1$ , resulting in  $u(\mathbf{x}, t) \approx 0$  for  $t > t_1$ . Now suppose that some external process deposits packets of concentration at random times  $t$  that form a homogeneous Poisson process, and let  $u_\Sigma(\mathbf{x}, t)$  represent the linear sum of the decaying concentrations arising from all of the deposited events. Finally, suppose that secondary events occur in a random fashion, with the generation probability of an event at a particular time  $t$  and location  $\mathbf{x}$  proportional to the accumulated concentration  $u_\Sigma(\mathbf{x}, t)$  at that time and location, independent of other generated events.

**10.8.1.** Show how the fractal-shot-noise-driven Poisson process provides a useful model for the resulting secondary event process.

**10.8.2.** What values of  $\beta$  are likely operative? What dimensionality leads to exact  $1/f$  noise?

**10.8.3.** Demonstrate how the approach can be generalized to the case where the packets arrive at different points  $\mathbf{x}$ , and need not all have the same initial concentration  $u_0$ .

**10.8.4.** Provide an example of how physical constraints can make diffusion unrealistic as a model even though it yields a mathematically plausible fractal exponent.

**10.9 Semiconductor high-energy particle detectors** A typical high-energy particle detector consists of a lightly doped  $p$ - $n$  junction with a large reverse bias voltage applied across it (Knoll, 1989). Energetic charged particles enter the detector, usually along the  $p$ - $n$  axis, and create electron-hole pairs within a large part of the semiconductor depletion region. The higher the energy of the particle, the greater the number of electron-hole pairs produced. The high reverse-bias field then sweeps these carriers out of the depletion region of the diode, electrons toward the  $n$  region and holes



toward the  $p$  region. This occurs before many of the electrons and holes recombine although some of the carriers do recombine, thereby reducing the detected charge created by the original energetic charged particle. A description of the recombination process therefore proves useful.

Consider a single energetic particle entering the detector at time  $t = 0$ . Assume that the electron-hole pairs are created instantaneously throughout the semiconductor depletion region, distributed as a three-dimensional Poisson point process, and that they begin diffusing immediately after their creation. Whenever an electron and a hole approach within some critical radius, the two carriers either recombine, thereby annihilating each other immediately, or first form an exciton and later recombine. In either case the carriers no longer carry current and effectively vanish.

**10.9.1.** If we ignore the drift current, with what exponents do the concentrations of electrons and holes decay?

**10.9.2.** How does drift affect the exponents?

**10.9.3.** Cast the recombination process in terms of an impulse response function.

**10.9.4.** Finally, show how the fractal-shot-noise-driven Poisson process may help in understanding the total recombination process in a working particle detector.

**10.10** *Trapping in amorphous semiconductors: Revisited* An alternative approach to the problem of trapping in amorphous semiconductors, initially considered in Prob. 7.10, treats all conductance changes as events in an auxiliary point process (Azhar & Gopala, 1992). Analysis of current flow in an AC128 germanium transistor reveals relatively fast current fluctuations during conduction events, separated by somewhat longer intervals between conduction events. For a fixed counting time, the mean and variance of the numbers of conduction-event onsets assume similar values; the same holds for the numbers of conductance changes within a conduction event. Furthermore, all the secondary events taken together, which form the auxiliary point process, have a spectrum that follows a  $1/f$ -type form. Considering the evidence presented, suggest a plausible model for the sequence of conductance-change events.